

# The long-term circulation driven by density currents in a two-layer stratified basin

By M. G. WELLS<sup>1,†</sup> AND J. S. WETTLAUFER<sup>1,2</sup>

<sup>1</sup>Department of Geology and Geophysics, Yale University, New Haven, CT 06520-8109, USA

<sup>2</sup>Department of Physics, Yale University, New Haven, CT 06520-8109, USA

(Received 20 May 2005 and in revised form 21 July 2006)

Experimentation and theory are used to study the long-term dynamics of a two-dimensional density current flowing into a two-layer stratified basin. When the initial Richardson number,  $Ri_\rho^{in}$ , characterizing the ratio of the background stratification to the buoyancy flux of the density current, is less than the critical value of  $Ri_\rho^* = 21 - 27$ , it is found that the density current penetrates the stratified interface. This result is ostensibly independent of slope for angles between  $30^\circ$  and  $90^\circ$ . If the current does not initially penetrate the interface, then it slowly increases the density of the top layer until the interfacial density difference is reduced sufficiently to drive penetration. The time scale for this to occur,  $t_p = (Ri_\rho^{in} - Ri_\rho^*)L/B^{1/3}$ , is explicitly a function of the buoyancy flux  $B$  and the length of the basin  $L$ . The initial Richardson number,  $Ri_\rho^{in}$ , is a function of depth, the initial reduced gravity of the interface and a weak function of slope angle. In the absence of initial penetration for very steep slopes of  $75^\circ$  and  $90^\circ$ , we observe that penetrative convection at the interface leads to significant local entrainment. In consequence, the top layer thickens and the interfacial entrainment rate increases as the fifth power of the interfacial Froude number. In contrast, such a process is not observed at comparable interfacial Froude numbers on lower slopes of  $30^\circ$ ,  $45^\circ$  and  $60^\circ$ , thereby demonstrating the important role of impact angle on penetrative convection. We attribute the increased interfacial entrainment by the steep density currents as the result of the transition from an undular bore to a turbulent hydraulic jump at the point where the density current intrudes. We discuss the applicability of the observed circulation to the stability of the Arctic halocline where we find  $0.56 \lesssim t_p \lesssim 1.2$  years for a range of contemporary oceanographic conditions.

---

## 1. Introduction

Cooling in the shallow shelf regions of lakes and polar seas, or evaporation in marginal seas, leads to the formation of dense water masses that become cascading density currents. In many cases, the source water in such currents is denser than the bottom waters of the basin into which it flows, but mixing due to shear instabilities dilutes the current so that it can intrude at mid-depth, as is the case for the Mediterranean outflow (Baringer & Price 1999). In stratified lakes and reservoirs, inflow of a cold river or differential cooling in shallow regions also results in the

† Present address: Department of Physical and Environmental Sciences, University of Toronto at Scarborough, Toronto ON M1C 1A4, Canada.

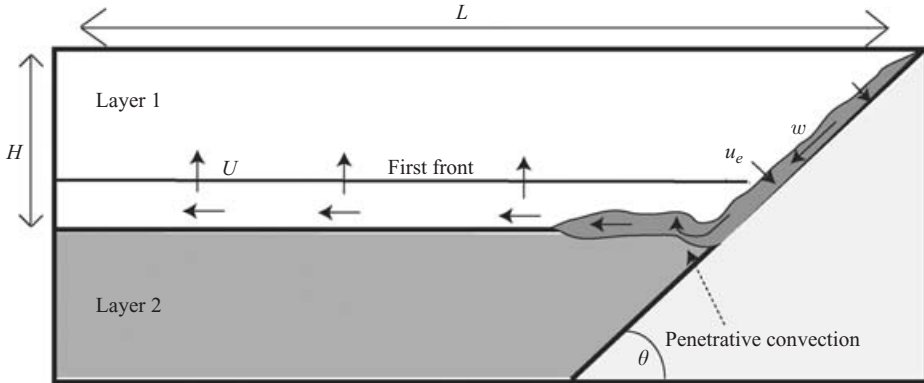


FIGURE 1. A density current flowing down a slope with velocity  $w$  will dilute owing to turbulent entrainment of the lighter fluid above. If there has been sufficient dilution, then the density current will initially spread out along the interface as a thin intrusion, similar to the experiments of Monaghan *et al.* (1999). The subsequent input of fluid deepens the pool of dense water that forms above the interface, as previously described by Wells & Wettlaufer (2005). The upper layer continues to become more dense, decreasing the interlayer buoyancy contrast until the density current penetrates through the interface. After penetration, the volume flux out of the upper layer thickens the lower layer.

formation of density currents. The stratification of such fresh-water basins can often be approximated by a two-layer stratification, with a well-mixed warm surface layer (the ‘epilimnion’) separated by a sharp thermocline from the deeper cold waters (the weakly stratified ‘hypolimnion’). When a density current enters such a two-layer stratification, there are two possible outcomes: if the impinging current is lighter than the lower layer then an intrusion forms on the thermocline as sketched in figure 1; otherwise, it will intrude at the very base of the reservoir. These two possibilities have long been recognized by limnologists who use the terminology of an ‘interflow’ for the subsurface intrusion, and ‘underflow’ to refer to a density current spreading along the base (Fischer *et al.* 1979; Hebbert *et al.* 1979; Imberger & Hamblin 1982). An important application of our work concerns the buoyancy forcing in the Arctic oceans driven by seasonal freezing and melting. The rejection of brine from growing sea-ice on the shallow shelf regions of the Arctic ocean leads to sinking density currents that interact with the Arctic halocline, and it is important to know how stable this circulation pattern is to possible changes in either the buoyancy forcing or the halocline strength.

The layer into which the density current intrudes is a function of the initial buoyancy flux, the density jump across the thermocline and how much mixing occurs on the slope before it reaches the depth of the thermocline. The level at which a buoyant plume intrudes in a continuously stratified environment was first quantified in terms of entrainment rates in the seminal work of Morton, Taylor & Turner (1956). They found that in a linear stratification, the height of rise of a point-source plume is a simple function of the initial buoyancy flux and ambient stratification. Briggs (1969) confirmed the validity of the Morton *et al.* (1956) scaling over five orders of magnitude: from the laboratory scale to large oil fires. The central assumption in this theory is the ‘entrainment hypothesis’ of G. I. Taylor (1948), whereby the rate at which the rising fluid turbulently entrains surrounding ambient fluid is assumed to be linearly proportional to the mean vertical (axial) velocity,  $w$ , which is often expressed in terms of an entrainment ratio

$$E = u_e/w, \quad (1)$$

where  $u_e$  is the entrainment velocity normal to the current. For a plume, the entrainment ratio is constant and equal to 0.1, but for a density current the entrainment ratio decreases as the stability of the current increases. The use and development of this assumption, and the distinctions between definitions and nomenclature are discussed in detail by Turner (1986). Armed with the entrainment assumption, Morton *et al.* (1956) were able to solve ordinary differential equations for the mass, momentum and buoyancy fluxes in the case where a point source of buoyancy enters a linearly stratified unconfined environment. The height to which a two-dimensional buoyancy source will rise in a linear stratification was considered by Wright & Wallace (1979) and Bush & Woods (1999), and the effect of nonlinear stratification was investigated by Caulfield & Woods (1998). Of most relevance to the case where a two-dimensional density current enters a two-layer stratified reservoir are the experiments of Wallace & Sheff (1987) and Ching, Fernando & Noh (1993).

The long-term effect of a density current flowing into a confined basin will be to increase the basin density gradually. The density current modifies the basin stratification through the ‘filling-box’ dynamics of Baines & Turner (1969), whereby the outflow of the plume continuously upwells and is re-entrained into the density current. This forms a stable stratification, with a transient evolution described by Worster & Huppert (1983). Cardoso & Woods (1993) investigated how a point-source plume modifies a linear stratification in a confined basin. They found that the plume initially spreads at the level predicted by Morton *et al.* (1956). Thereafter, above the level of intrusion, the entrainment by the plume forced the same circulation and stratification as the filling box model, while the level at which the plume intruded deepened owing to entrainment by penetrative convection at the base of the plume. The long-term dynamics of a point source of buoyancy in a confined two-layered stratification were studied by Baines (1975) and Kumagai (1984), who showed that the entrainment due to penetrative convection at the density interface deepens the upper layer and thereby modifies the density distribution of the Baines & Turner (1969) model, which has an impermeable lower boundary (see for example figure 4 of Baines 1975). If the negatively buoyant plume does not initially penetrate the interface, then the buoyancy contrast between the two layers decreases in time by a filling-box process in the upper layer, and the density current eventually penetrates to the bottom of the basin. Kumagai (1984) determined the time scale over which the buoyancy contrast is sufficiently reduced that penetration of the interface occurs. This critical buoyancy contrast is similar to that discussed by Wallace & Sheff (1987) and Ching *et al.* (1993).

There are many lakes or oceanic basins that have dynamics similar to the filling-box model of Baines & Turner (1969). Examples where modified versions of the filling-box model have been used include Killworth & Carmack (1979) and Hamblin & Carmack (1978) who looked at the seasonal variation caused by a dense river inflow into the Kamloops lakes in Canada; and Sukru, Ozsoy & Unluata (1993) who modelled the seasonal stratification of the Marmara Sea where there is lower-layer inflow from the Dardanelles. In a related study, Wells & Sherman (2001) examined the formation of upwelling due to a density current in the Chaffey Reservoir in Australia. The overturning circulation in the World’s oceans, where dense water forms and sinks at high latitude and then upwells through the main thermocline at lower latitudes, was described first by Stommel (1958) and by many others since then, the most recent variants of this concept being given by Hughes & Griffiths (2006) and Wahlin & Cenedese (2006). An assumption underlying all of these models is that the (weak) entrainment into a density current will result in the same filling-box dynamics as the

strongly entraining vertical plumes. The relationship between entrainment in plumes and jets and density currents on slopes is discussed by Ellison & Turner (1959). In their treatment of overturning circulation, Hughes & Griffiths (2006) pointed out that the small along-slope entrainment rates into density currents on a slope can be viewed in terms of the entrainment rate per unit height of fall, and by interpolating the entrainment rates for slopes between  $0^\circ$  and  $5^\circ$ , they found values comparable to those for a vertical free plume. This prediction is confirmed in the laboratory experiments of Wells & Wettlaufer (2005). Therefore, observed upwelling velocities and density profiles driven by two-dimensional density currents in confined basins are essentially the same as theoretical predictions for those driven by a buoyant line source in two-dimensional filling boxes, as described Baines & Turner (1969).

In this paper, we quantify the conditions necessary for a two-dimensional density current on a slope to penetrate through a two-layer stratification. In §2 we use the observations of Wells & Wettlaufer (2005) to extend the theory of Wallace & Sheff (1987) and Ching *et al.* (1993) and thereby determine the critical buoyancy step required to stop penetration of a density current as a function of the vertical distance the density current descends and the buoyancy flux. For cases where the density current does not initially penetrate the interface, we determine (i) the time scale  $t_p$  over which the density current reduces the buoyancy step to the critical value, and (ii) the resulting stratification and circulation. A description of the experiment is given in §3.1 and observations of the circulation, the critical buoyancy step, the time scales to penetration, and the observed entrainment at the interface are presented in §3.2. Finally, in §4, we discuss applications of this to the dynamics and stability of the Arctic halocline.

## 2. Theory

### 2.1. Interaction of plumes and density interfaces

For the case of a point-source plume, Morton *et al.* (1956) quantified the role of entrainment in determining how an initially dense plume dilutes with distance from the source. The same is the case for a two-dimensional plume or a density current. Depending on the relative densities, a buoyant plume or density current can be blocked by a two-layer stratification. The conditions for penetration or blockage have been explored experimentally by studying the impingement of a two-dimensional plume upon a sharp density interface at a depth  $H$  below the source with buoyancy flux per unit width,  $B$  ( $[B] = \text{m}^3 \text{s}^{-3}$ ) and a reduced gravity of the density step defined as  $\Delta_{12} = g(\rho_2 - \rho_1)/\rho_o$ , where  $\rho_1$  and  $\rho_2$  are the densities in the upper, 1, and lower, 2, layers,  $\rho_o$  is a reference density and  $g$  is the acceleration due to gravity (Wallace & Sheff 1987; Noh, Fernando & Ching 1992; Ching *et al.* 1993). Ostensibly the same result is found in these studies with the earlier work determining, in particular, that the plume penetrates the density step when  $(H\Delta_{12})/B^{2/3} < 3$  and it is blocked by the interface and spreads laterally at the depth of the interface when  $(H\Delta_{12})/B^{2/3} > 7.8$ . Ching *et al.* (1993) studied the conditions for a negatively buoyant line plume to penetrate a two-layer interface based on the vertical velocity at the interface  $w$ , the reduced gravity  $\Delta_{12}$  and the thickness  $b$  of the plume at the density front. Together these variables define a Richardson number,

$$Ri = b\Delta_{12}/w^2, \quad (2)$$

which can be related to a Froude number, of the flow by  $Ri = Fr^{-2}$ . By varying this Richardson number, Ching *et al.* (1993) identified different flow patterns. When

$Ri < 0.5$ , the plumes penetrate through the interface into the lower layer, whereas for  $1 < Ri < 5$ , the plumes spread laterally at the interface with appreciable entrainment of dense underlying fluid occurring at a rate that decreased with increasing Richardson number (Ching *et al.* 1993, figures 9 and 10). When  $Ri > 10$ , little mixing was observed. A subtly different form of the Richardson number was defined by Wallace & Sheff (1987) as

$$Ri_\rho \equiv \Delta_{12} H / B^{2/3}. \quad (3)$$

Whereas equation (2) can be thought of as a ratio of potential to kinetic energies, the form of Richardson number used by Wallace & Sheff (1987) is an expression of the density excess.

By considering the scalings for the width, velocity and density anomaly of a free two-dimensional plume, our results and those of Wallace & Sheff (1987) and Ching *et al.* (1993) can be placed in the same context. The plume scalings are

$$b = 2Ez, \quad (4)$$

$$w = 2^{-1/3} E^{-1/3} B^{1/3} \quad (5)$$

$$\Delta = 2^{1/3} E^{-2/3} B^{2/3} z^{-1}, \quad (6)$$

with  $\Delta$  the buoyancy (reduced gravity) of the plume,  $z$  the vertical distance and  $E$  the entrainment ratio of the plume (Morton *et al.* 1956; Turner 1973). Hence at the interface where  $z = H$ , equation (3) can be combined with (4) and (5) to show that  $Ri = (2E)^{5/3} Ri_\rho$ . Hence, for a given entrainment coefficient, the density and energy criteria used by Ching *et al.* (1993) and that of Wallace & Sheff (1987) are equivalent.

Consider now the case when the buoyancy of the plume relative to the upper layer is the same as the buoyancy jump across the interface and hence  $\Delta = \Delta_{12} \equiv \Delta_{12}^{crit}$ , and the plume can penetrate the interface at  $z = H$ . Whence, in terms of density we have

$$Ri_\rho^{crit} \equiv \Delta_{12}^{crit} H / B^{2/3} = 2^{1/3} / E^{2/3}, \quad (7)$$

and when  $E = 0.1$  this implies that  $Ri_\rho^{crit} = 5.8$ , in good agreement with that observed by Wallace & Sheff (1987). Because  $Ri^{crit} = 0.069 Ri_\rho^{crit}$ , the observation of Noh *et al.* (1992) that  $Ri^{crit} = 0.5$ , shows the experimental agreement between the energy and density criteria for penetration.

## 2.2. Relationship between density currents and plumes

The relationship between the results discussed above, from vertical two-dimensional plumes, and two-dimensional density currents on a slope is established by considering the nature of entrainment in these two geometries. Density currents on slopes are often characterized in terms of an overall Richardson number,  $Ri_o$ , which describes the stabilizing effect of the density gradient relative to the shear as

$$Ri_o = \frac{b \Delta \cos \theta}{w^2}, \quad (8)$$

for currents of thickness  $b$ , reduced gravity  $\Delta$ , and mean velocity  $w$  on a slope of angle  $\theta$  (Ellison & Turner 1959; Turner 1973, 1986; Baines 2005). In the theory of Ellison & Turner (1959), the entrainment ratio, or entrainment constant,  $E_s$ , is defined in terms of the rate of increase in the density current thickness as a function of distance down slope, whereas for a vertical plume, the entrainment ratio is the rate of increase in horizontal plume width as a function of depth,  $E$ . (We note here that in the original Morton *et al.* (1956) theory, the entrainment constant for a vertical plume is  $\alpha$  and Ellison & Turner (1959) actually use the notation  $E$  for the slope-dependent

entrainment ratio and in our previous work we followed their convention (Wells & Wettlaufer 2005). Here we use  $E$  to describe the entrainment in vertical line or point plumes. In the literature we find that the same variable is used to describe several types of entrainment constant. Hence, herein we would like to make clear the distinction between the definitions.) When bottom friction and the pressure gradient associated with changes in  $b$  are less important than the stress associated with entrainment, mass and momentum conservation yield  $E_s = Ri_o \tan \theta$  (Turner 1973) from which it can be seen that,

$$\frac{E_s}{\sin \theta} = Ri, \quad (9)$$

with  $Ri$ , with the necessary changes having been made, given by equation (2).

If the one-sided nature of entrainment in a density current on a slope is related to that of a vertical plume, then we can define an equivalent vertical entrainment constant, which we denote as  $E_{eq}$ . Hughes & Griffiths (2006) showed that by making the simple coordinate transformation from along-slope position to vertical depth, that the two types of entrainment are simply related by

$$E_{eq} = \frac{E_s}{\sin \theta}. \quad (10)$$

Thus, the entrainment into a density current on a vertical slope is equivalent to that into a free plume. The experiments of Ellison & Turner (1959) are consistent with  $E_s \rightarrow 0$  as the slope tends to zero, and Hughes & Griffiths (2006) assumed a linear interpolation between the measured value at laboratory slopes,  $E_s = 10^{-2}$  at  $\theta = 5^\circ$ , and the zero slope limit  $E_s \rightarrow 0$ . They concluded that at low slope angles,  $E_{eq}$  would asymptote to 0.1, the approximate value of a vertical plume. Hence currents on small slopes entrain at a rate (per unit height) comparable to that for a vertically falling plume distant from boundaries. Wells & Wettlaufer (2005) have shown experimentally that over a wide range of angles below approximately  $80^\circ$ ,  $E_{eq}$  takes a constant value of 0.08.

For a two-dimensional gravity current on a slope, Britter & Linden (1980) showed that the equations for the current thickness, velocity and buoyancy are almost the same as equations (4)–(6), but with a slope dependent entrainment rate, namely,

$$b = E_s s, \quad (11)$$

$$w = C E_s^{-1/3} B^{1/3}, \quad (12)$$

$$\Delta = C^{-1} E_s^{-2/3} B^{2/3} s^{-1}, \quad (13)$$

where  $s$  is the along slope distance. The factor  $C$  has been experimentally determined by Ellison & Turner (1959) to be  $C = 0.2$  for slopes between  $10^\circ$  and  $90^\circ$ . We can determine a condition similar to equation (7) by using the equivalent entrainment rate  $E_{eq} = 0.08$  and the vertical depth of the descent of the density current  $H = s \sin \theta$ . Then the critical value becomes

$$Ri_\rho^* \equiv \Delta_{12}^{crit} H / B^{2/3} = C^{-1} E_{eq}^{-2/3} (\sin \theta)^{1/3}. \quad (14)$$

Considering the range of  $\theta$  from  $30^\circ$  to  $90^\circ$  used in our experiments, the right-hand side of equation (14) shows that  $21 \leq Ri_\rho^* \leq 27$ , and hence the critical value for penetration is a very weak function of slope. Because of the slightly slower velocity of density currents relative to free plumes, and the fact that they entrain on only one side, it is the case that for the same buoyancy flux  $B$  there is less dilution with depth. Thus for the same  $H$ , the critical buoyancy step at the interface must be greater than

that of the free plume case studied by Wallace & Sheff (1987), Noh *et al.* (1992) and Ching *et al.* (1993). We describe a test of these conclusions for density currents on slopes between  $30^\circ$  and  $90^\circ$  in §3.2.

### 2.3. Density and velocity profiles of the surroundings

If the density current does not penetrate the interface, then the upper layer evolves by the filling-box mechanism. The conservation equations for volume, momentum and density deficiency in a two-dimensional line plume are discussed in detail in Baines & Turner (1969) and Wells & Wettlaufer (2005). The important results for the present discussion are the form of the upwelling velocity  $U$  and the environmental density  $\Delta_o(z)$ . It is observed that the mean velocity of a two-dimensional steady turbulent density current is constant (Ellison & Turner 1959) and hence for a constant entrainment coefficient, the thickness of the current grows linearly with depth as  $b = Ez$ . The equation of continuity is that  $-LU = bw$  where  $L$  is the basin length, which is constant with depth in the following. This leads to an upwelling velocity that is also a linear function of depth;  $U = -zEw/L$ . Such an upwelling velocity implies that the position  $\zeta$  of density fronts for a filling box produced by a density current on a slope varies with time as

$$\zeta = \exp(-\tau), \quad (15)$$

where the non-dimensional time is defined through  $t = 2^{2/3} B^{-1/3} E_{eq}^{-2/3} L \tau$ , in which we have used the equivalent entrainment constant  $E_{eq}$ , and the non-dimensional depth is given by  $\zeta = z/\hat{H}$ . Here,  $\hat{H}$  is the slowly varying depth of the stratified region, which is initially the same as the depth  $H$  of the line-source above the interface. The upper-layer depth  $\hat{H}$  may increase with time owing to interfacial entrainment, but if  $\partial \hat{H} / \partial t \ll U$ , then equation (15) holds to a good approximation. We verify this condition experimentally.

In our experiments, the density of the environment changes only because of vertical advection  $U$ , so that

$$\frac{\partial \Delta_o}{\partial t} = -U(z) \frac{\partial \Delta_o}{\partial z}. \quad (16)$$

For times long in comparison to the time at which the first front has reached the top of the basin, as in the original Baines & Turner (1969) model, the asymptotic state is reached in which the environmental density slowly increases with time, but the shape of the density profile is unchanged. This environmental density profile is achieved by combining a linear upwelling velocity with equation (16) to yield

$$\Delta_o = \ln(\zeta) + \tau, \quad (17)$$

where the dimensionless buoyancy of the environment is defined through  $\Delta_o = 2^{-1/3} B_o^{2/3} E_{eq}^{-2/3} \hat{H}^{-1} \Delta_o(\zeta, \tau)$ . The time constant in equation (17) is evaluated using the fact that the total buoyancy in the tank increases at a rate determined by buoyancy flux normalized by tank volume.

### 2.4. Deepening of the upper layer

The interface between the upper and lower layers in figure 1 is the moving boundary through which the entrainment of dense lower-layer fluid takes place, as discussed by Baines (1975) and Kumagai (1984). As this interface deepens, local interfacial

entrainment increases the density of the fluid in the outflow. The entrainment velocity  $U^*$  is defined by

$$U^* = \frac{\partial \hat{H}}{\partial t}. \quad (18)$$

Baines (1975) and Kumagai (1984), described the entrainment velocity  $U^*$  at such a sharp two-layer interface in terms of a Froude number of the density interface, which is a function of the local thickness  $b$ , velocity  $w$  and reduced gravity  $\Delta$  of the outflowing fluid. In order to make contact with their work and others, we use the same notation but note that this is equivalent to a characterization in terms of a Richardson number as described in equation (2), namely,  $Fr_{int} = Ri^{-1/2}$ . Hence, if  $L$  is the length of the tank,

$$\frac{LU^*}{bw} = f(Fr_{int}), \quad (19)$$

and equation (18) can be rewritten to describe the increase in thickness of the upper layer as

$$\frac{\partial \hat{H}}{\partial t} = \frac{bw}{L} f(Fr_{int}). \quad (20)$$

In experiments with point-source plumes, Baines (1975) found the entrainment volume flux varied as  $Fr_{int}^3$ . Kumagai (1984) found the same result at low Froude numbers, but showed that the entrainment rate approached a constant as  $Fr_{int} \rightarrow 1$ . In experiments where a line source of buoyancy impinged upon a two-layer interface, Ching *et al.* (1993) measured the entrainment velocity for a limited number of data points and found a power law of the form  $LU^*/wb = 0.6Fr_{int}^2$  for  $0.1 < Fr_{int} < 1$ . The critical Froude (and Richardson) number implied by (7) provides an upper bound on the entrainment rate. Using continuity ( $-LU = bw$ ) and the results of Ching *et al.* (1993), the ratio of the entrainment velocity to the filling box upwelling velocity varies as  $U^*/U \propto Fr_{int}^2 = Ri^{-1}$ . This ratio is very small for small  $Fr_{int}$  (large  $Ri$ ), justifying the assumption that the interface depth can be considered constant over the time during which the density and velocity profiles evolve in the upper layer. The Froude number for penetrative convection at a density interface is defined as  $Fr_{int} = w_z/\sqrt{b_x \Delta_{12}}$ , where  $w_z$  is the vertical component of the velocity and  $b_x$  is the horizontal thickness. The scaling of equation (9) gives the horizontal thickness of the density current as  $b_x = E_{eq} \sin \theta^{-1} H$ , and the vertical component of the velocity of the density current as  $w_z = CE_{eq}^{-1/3} B^{1/3} \sin \theta^{2/3}$ . Hence, the Froude number at an interface of depth  $\hat{H}$  is,

$$Fr_{int} = C(\sin \theta)^{5/6} E_{eq}^{1/6} \frac{B^{1/3}}{\sqrt{\hat{H} \Delta_{12}}}, \quad (21)$$

where initially  $Fr_{int} = C(\sin \theta)^{5/6} E_{eq}^{1/6} \times (Ri_\rho^{in})^{-2}$ .

The total buoyancy in the upper layer, 1, owing to input of buoyancy from the plume and from the additional entrainment at the base, is

$$\int_0^{\hat{H}} L \frac{\partial \Delta_1}{\partial t} dt = B + B^*, \quad (22)$$

where  $B^* = L\Delta_{12}U^*$  is the additional buoyancy flux per unit length owing to mixing across the interface. If the density is changing at the same rate at all levels within the upper layer (as assumed in Baines & Turner 1969; Wells & Wettlaufer 2005)



then

$$\frac{\partial \Delta_1}{\partial t} = \frac{B + B^*}{L \hat{H}}. \quad (23)$$

Integrating (23) and re-arranging gives

$$\Delta_1(t) = \frac{1}{1 - \partial \ln \hat{H} / \partial \ln t} \frac{Bt}{L \hat{H}} + \frac{\Delta_{12}^m}{\hat{H}(t)} \frac{\partial \hat{H}}{\partial t} t. \quad (24)$$

When there is no deepening of the upper layer owing to entrainment,  $\hat{H} = H$  and this reduces to  $\Delta_1(t) = Bt/LH$ . Using (24) and the experimentally observed  $\partial \hat{H} / \partial t$ , we can estimate (a) the change in density of the upper layer, (b) the Froude number and (c) the entrainment flux  $B^* = L \Delta_{12} U^*$ . In equation (24),  $B$  is independent of time, but due to mixing across the interface, the buoyancy step  $\Delta_{12}$  decreases with time, and thus  $B^*$  is predicted to increase with time. The depth also increases with time owing to the entrainment by penetrative convection at the interface. For the simple case where  $B^* = 0$ , the depth  $\hat{H}$  is constant and we can integrate equation (23) to determine the time,  $t_p$ , over which the initial reduced gravity  $\Delta_{12}^m$  is decreased to that of the critical buoyancy step  $\Delta_{12}^{crit}$  defined by equation (14). Whence, we find the penetration time to be

$$t_p = \frac{(R_i^m - R_i^*)L}{B^{1/3}}. \quad (25)$$

For cases where there is significant entrainment at the interface, the fact that both  $B^*$  and the upper-layer depth increase with time, means that the ratio on the right-hand side of equation (23) remains approximately constant. We will show later (see figure 4) that equation (25) is a very good estimate for the time to penetration, even for cases where significant deepening occurs, and provides a very useful model for the Arctic halocline.

The vertical distribution of density in the upper layer is given by

$$\frac{\partial \Delta_1}{\partial z} = \frac{B + B^*}{bw \hat{H}}. \quad (26)$$

The velocity  $w$ , and thickness  $b$  of the density current or plume are not affected by the penetrative convection at the interface. If we again assume that the rate of change of  $\hat{H}$  is much smaller than the upwelling filling box velocity, then the density profile has the same shape as (17), but the magnitude is increased by the factor  $1 + B^*/B$ . Our results in §3.2 show that the maximum values of  $1 + B^*/B$  are 1.25. The energy arguments of Manins & Turner (1978) imply that the ratio of buoyancy fluxes  $B^*/B$  must be less than 0.5, as found by Kumagai (1984).

### 3. Laboratory experiments

#### 3.1. Description of experiment

A total of 22 experiments were performed in a geometry similar to that shown in figure 1. The tank has a length  $L = 244$  cm, width of 15 cm and total depth of 45 cm. A ramp down which the density currents flow is set at one end, and the slope is set to  $30^\circ$ ,  $45^\circ$ ,  $60^\circ$ ,  $75^\circ$  or  $90^\circ$ . Owing to the length of the tank, the sloping boundaries contribute little to the total available volume. We prepare a two-layer salt stratification with a lower layer of thickness 17 cm and an upper fresher layer of thickness 22 cm. The initial salinity difference is determined using a refractometer. This fixes the initial buoyancy step  $\Delta_{12}^m$ . Density currents are produced by pumping

Run	Slope	$\Delta_{12}^{in} \text{ cm s}^{-2}$	$Ri_{\rho}^{in}$	$t_p$ , theory (s)	$t_p$ , observed (s)
1	45°	7.54	22.83	0	0
2	45°	12.54	37.96	991–1535	1230–1675
3	45°	20.97	63.46	3300–3842	2500–3000
4	45°	27.34	82.74	5044–5587	3750–4500
5	45°	35.08	106.17	7163–7708	6080–7485
6	60°	6.95	21.05	0–5	0–100
7	60°	12.39	37.37	938–1481	1630–2790
8	60°	20.26	61.39	3112–3655	2500–3200
9	60°	26.65	80.67	4857–5400	3500–4000
10	75°	39.39	119.22	8346–8889	7000–8000
11	75°	14.014	42.41	1394–1937	1680–2010
12	75°	20.972	63.46	3300–3843	3200–4000
13	75°	9.11	27.58	52–595	560–870
14	90°	39.39	119.22	8346–8889	8270–8600
15	90°	15.09	45.67	1689–2232	2300–2500
16	90°	8.33	25.20	0–380	720–1150
17	Free plume	8.33	25.20	0–380	NA
18	Free plume	2.45	7.41	0	NA
19	Free plume	25.18	76.22	4454–4997	NA
20	Free plume	19.21	50.71	2146–2689	NA
21	30°	25.18	76.22	4454–4997	3000–4000
22	30°	15.38	46.56	1770–2313	1500–2500

TABLE 1. Experimental parameters. For runs 17–20, the entrainment at the interface deepened the upper layer to the base of the tank before the plume penetrated through the interface, and hence no experimental  $t_p$  are given. Significant increases in the depth of the upper layer (greater than 1 cm) were seen only in runs 10–20. In calculating the range of times to penetration  $t_p$  from (25), we use the measured value of  $Ri_{\rho}^{in}$ , a value of  $Ri_{\rho}^*$  of 21 and 27,  $L = 244$  cm and  $B = 19.6 \text{ cm}^3 \text{ s}^{-3}$ . A discussion of the range of observed  $t_p$  is given at the end of § 3.2.

a saturated saline solution of density  $\rho = 1.199 \text{ g cm}^{-3}$  at a rate of  $Q = 1.5 \text{ cm}^3 \text{ s}^{-1}$  through a two-dimensional manifold located 1 cm above the slope, and at a height of 22 cm above the interface between the fresh upper layer and the lower saline layer. The buoyancy flux per unit width is then  $B = 19.6 \text{ cm}^3 \text{ s}^{-3}$ . Both the buoyancy flux  $B$  and the height  $H$  of the line source above the density interface are held constant, so that  $Ri_{\rho}^*$  described by equation (14) is experimentally controlled by  $\Delta_{12}^{crit}$ . We predict a range of  $Ri_{\rho}^* = 21 - 27$ . The initial buoyancy contrast between the two layers is varied so that the ratio  $Ri_{\rho}^{in}/Ri_{\rho}^*$  is varied from a value of unity to five. The experimental parameters are shown in table 1.

The principal quantitative observation is the time at which the density current penetrates the density interface. By periodically introducing dyes of different colours into the density current, we monitor (a) the depth of the outflow and (b) the position of the initial density front between the two layers as a function of time (figure 2). Digital photographs of the dye layers are taken every 10 s, from which we extract vertical image slices. These slices are stacked temporally, and the time history of the various stratified dye layers is shown in figure 3. The trajectories of dye lines in the time slices allow the vertical velocities within the tank to be quantified, in a similar manner to Wells & Wettlaufer (2005).

### 3.2. Experimental results

A typical experiment (run 5) is shown in figure 2, displaying the region of the tank within 90 cm of the dense current. The slope is 45° and the initial buoyancy step is

very large, so that  $Ri_\rho^{in}$  is almost five times the critical value of  $Ri_\rho^* = 21$ . Hence, in figure 2(a), we see that the density current initially spreads out along the interface as a thin intrusion. The subsequent input of fluid deepens the pool of dense water that forms above the interface (figure 2b), as previously described by Wells & Wettlaufer (2005). Note that the depth of the upper layer does not change between these two photographs, indicating that no penetrative convection has occurred where the plume impacts the buoyancy step. The input of dense fluid ensures that the upper layer continues to become more dense, so that the buoyancy contrast between the two layers decreases, until the density current penetrates through the interface to the base of the tank (figure 2c). After penetration of the interface, there is a volume flux out of the upper layer into the lower layer so that the latter thickens and the upper layer thins (figure 2d).

In figure 3, we plot time slices from three experiments that delineate the three possible outcomes of a density current impacting a stratified interface: (a) the density current initially penetrates the interface; (b) the density current penetrates after a period of time, before which there is no penetrative convection at the interface between the two layers or (c) there is strong penetrative convection at the interface and the upper layer deepens with time. In figure 3(a), we plot the time slice of run 1, in which  $Ri_\rho^{in} = 22.83 \sim Ri_\rho^* = 21$  and hence the density current almost immediately penetrates to the base of the tank and forces an upwelling within the lower layer. This is seen in the time slice by the rising interface that was originally located at a depth of 23 cm. Above this rising interface some of the dyed fluid is seen to detrain into the upper layer, while most of the density current penetrates to the base. In figure 3(b), we plot the time slice of run 5, for which individual photographs are shown in figure 2. As discussed above, this density current initially does not penetrate through the interface, and hence in the upper layer, we see the distinctive upwelling curves due to the filling-box process, described by  $\zeta = \exp(-\tau)$  in equation (15). The interface between the upper and lower layers does not change depth with time, indicating that there is no penetrative convection at the interface. Starting at approximately 4000 s through to 5500 s we see that a small fraction of dense fluid leaks through the interface into the lower layer, before the bulk of the dense current intrudes. This is because the current is not of uniform density, so the densest water parcels can penetrate before the bulk of the current. The density current penetrates through the interface, without detraining in the top layer, between 6080 and 7485 s, where the interface starts to upwell strongly. Because of the length of the period during which the density current detrains into both the top and bottom layers, it is slightly subjective what value of  $t_p$  to plot in figure 4; our decision to base this time scale on the time at which all of the dense current intrudes into the bottom layer may lead to a small but systematic overestimation of  $t_p$ . In figure 3(c), we plot the time slice of run 20, which is the case of a free plume. The lower interface deepens with time owing to penetrative convection beneath the plume, and the trajectory of this deepening upper layer is fitted numerically with the curve indicated, which we use later in evaluating  $\partial \hat{H} / \partial t$  in figure 5. As in figure 3(b), we see the characteristic upwelling curves of the filling box process (Wells & Wettlaufer 2005) described by equation (15).

We deduce that  $Ri_\rho^*$  is in the range of 21–27 by a best fit to equation (25) using the observed values of  $t_p$  and  $Ri_\rho^{in}$  from table 1 and plotted in figure 4. Such a critical value is in good agreement with that predicted by equation (14). However, as expected, this value is much larger than that found for two-dimensional vertical plumes as described by equation (7). This is because, for the same buoyancy flux, density currents have lower velocities than vertical two-dimensional plumes, and density currents remain

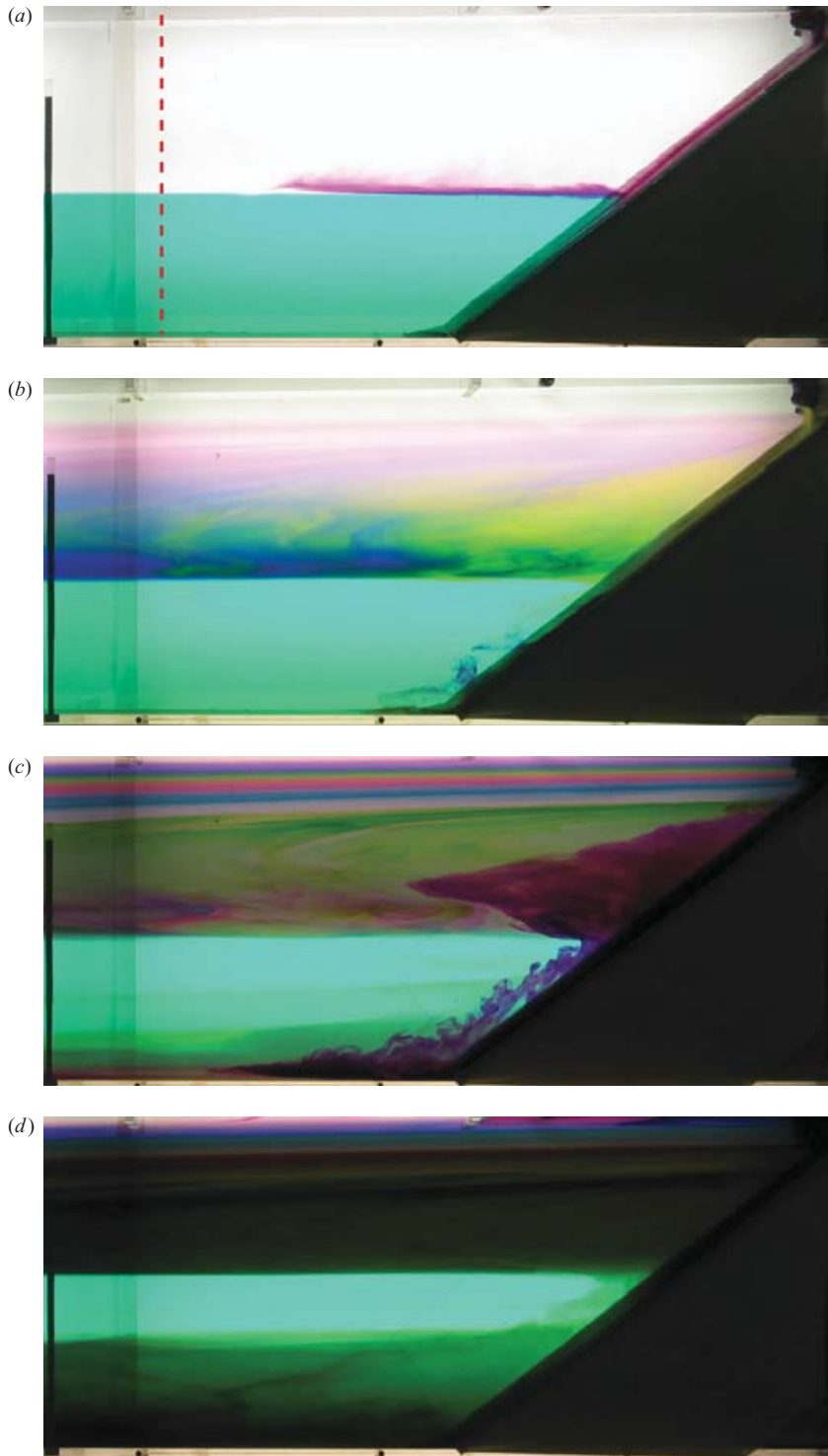


FIGURE 2. Photos from experiment 5 at times (a)  $t = 55$  s, (b)  $t = 1695$  s (c)  $t = 5760$  s and (d)  $t = 8000$  s. The tank is 240 cm long and only the 90 cm closest to the  $45^\circ$  slope are shown. The dotted red line in (a) shows the position at which data are taken to generate the times slices of figure 3(b).

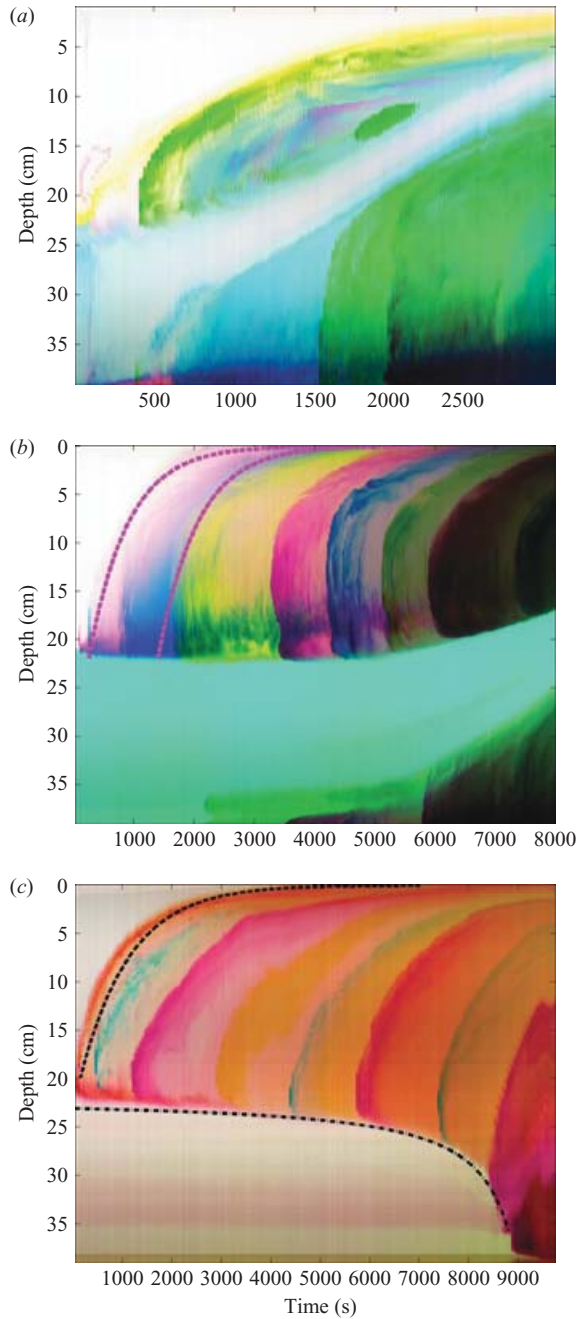


FIGURE 3. Time slices of runs 1, 5 and 20 taken at a vertical line 70 cm from the dense current. (a) Run 1. With a low initial buoyancy step so that  $Ri_\rho^{in} \sim Ri_\rho^*$ , the plume can initially penetrate through the interface and the lower-layer depth increases with time. (b) Run 5, also shown in figure 2. Because  $Ri_\rho^{in} \gg Ri_\rho^*$ , the density current does not initially penetrate the interface, and hence the upper layer shows characteristic filling-box dynamics, as indicated by plotting (15) against the observed interface trajectories. A small fraction of the dense fluid penetrates through the interface as early as 4000 to 5000 s, but the bulk of the density current intrudes only between 6080 and 7485 s. (c) Run 20. A free plume leads to penetrative convection at the interface and the upper layer deepens with time.

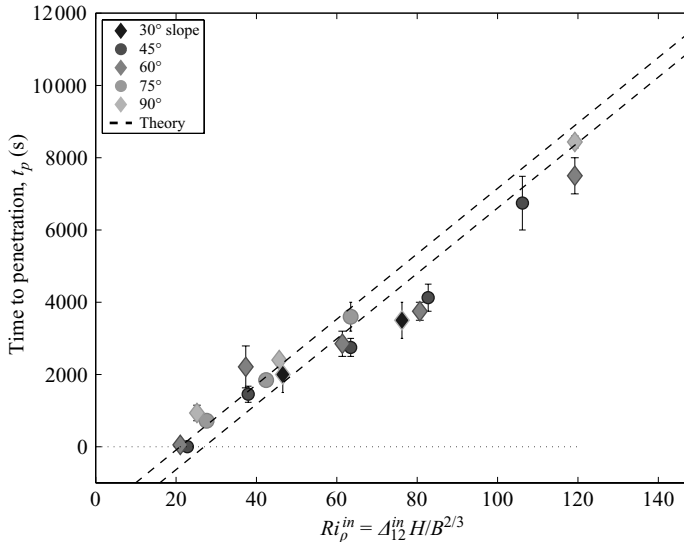


FIGURE 4. Experimental observations of the time until penetration,  $t_p$ , plotted against the initial value of the Richardson number,  $Ri_\rho^{in}$ . The time until penetration through the interface is simply the time it takes for the filling-box dynamics to reduce the upper interface contrast so that the critical density difference is reached. This can be seen to increase linearly with increasing  $Ri_\rho^{in}$ . The  $x$ -intercept of the line of best fit allows us to deduce that the value of  $Ri_\rho^*$  is between 21 and 27, and is in good agreement with the theoretical prediction of (14).

more dense because they can only entrain on one surface. The scatter in the data plotted in figure 4 is due to the difficulty of determining a well-defined penetration time. This is due to two effects. (i) Well before the bulk of the fluid penetrates, a small amount of very dense fluid starts to leak through the interface (figure 3*b*). This leakage is a result of the typical density current profiles (cf. Ellison & Turner 1959; Kneller, Bennett & McCaffrey 1999) which show greater velocity and density gradients than the better mixed vertical plumes. Because of the greater variation in the density within the current, there is a range of times over which penetration occurs, leading to the larger error bars for the lower-angle slopes in figure 4. (ii) On steeper slopes, greater than  $60^\circ$ , a related effect occurs, with the lighter well-mixed outer regions of the density current detrain at the interface after the bulk of the current has penetrated through the interface. Because of the variation in density within a turbulent plume or jet, part of the poorly mixed exterior of a jet has been observed to detrain at the density interface by a number of workers (Kulkarni, Murphy & Manohar 1993; Cotel & Breidenthal 1997; Monaghan *et al.* 1999; Baines 2001). For cases where fluid leaks through the interface before penetration, or fluid detrain at the interface after penetration, the details are sensitive to the gradients of velocity and density within the current.

### 3.3. Deepening of the upper layer

One of our most important observations is the lack of appreciable penetrative convection for density currents on slopes of less than  $75^\circ$ . We attribute this to a transition in the form of the hydraulic jump at the interface, from an undular bore to a turbulent bore (see e.g. Chow 1959). A hydraulic jump will occur when the density current on the slope changes from an entraining supercritical flow to a subcritical flow, which occurs when the density current intrudes into the two-layer stratification. The

form of the hydraulic jump will depend upon a Froude number of the density current, which is defined by Baines (1995) as  $Fr_o = Ri_o^{-1/2} = w/\sqrt{g'bw \cos \theta}$ , (with  $Ri_o$  given by equation (8)). For density currents on slopes between  $10^\circ$  and  $90^\circ$ , Ellison & Turner (1959) found that  $B/w^3 = 0.23 \pm 0.05$ . Combining this result with the conservation of buoyancy,  $B = g'bw$ , implies that the Froude number increases with the slope angle as  $Fr_o = (0.23 \cos \theta)^{-1/2}$ . The value of  $Fr_o$  on slopes greater than  $75^\circ$  will be greater than four, whereas experimental studies (Shin, Dalziel & Linden 2004; Marino, Thomas & Linden 2005) have found that density currents intruding into a stratified interior have a Froude number of about one. Hence, we expect that there will be a hydraulic jump condition between the supercritical slope case and the slower moving intrusion. Depending upon the initial value of  $Fr_o$ , this hydraulic jump may take the form of an undular bore (with little mixing or entrainment) or a turbulent bore (with significant mixing and entrainment). The relationship  $Fr_o = (0.23 \cos \theta)^{-1/2}$  implies that the strong turbulent mixing we observed for slopes greater than  $75^\circ$  initially occurs in the range from  $60^\circ$  to  $75^\circ$  and for Froude numbers of  $2.9 < Fr_o < 4$ . The fact that we observe such strong interfacial entrainment only at steep slopes where  $Fr_o > 2.9$  is consistent with Chow (1959). In his figure 15.2, he shows that for values of  $1 < Fr_o < 1.7$ , the classic undular hydraulic jump occurs with very little wave-breaking, whereas significant wave-breaking, and hence interfacial entrainment, starts to occur only in the range  $2.5 < Fr_o < 4.5$ . This explains why no mixing at the interface was observed in our experiments on slopes of  $30^\circ$ ,  $45^\circ$  and  $60^\circ$  for which the values of  $Fr_o$  were below 2.9. A similar sharp dependence of interfacial entrainment rates upon the incident angle was seen in the related experiments of Cotel *et al.* (1997), who found that the mixing efficiency of a jet striking a two-layer density interface was decreased dramatically when the jet was tilted by  $15^\circ$  from the vertical (i.e. at  $75^\circ$ ).

The entrainment that occurs at the interface between the two layers, for steep slopes, can be quantified in terms of an interfacial Froude number,  $Fr_{int}$ . The interfacial Froude number (equation (21)) decreases with slope angle, but in the experiments we also varied the initial values of  $\Delta_{12}$ , so that there were comparable values of  $Fr_{int}$  for both low- and high-angle slopes, thus making it unlikely that the transition between  $60^\circ$  and  $75^\circ$  in the normalized interfacial entrainment was due to changes in  $Fr_{int}$ . The observed normalized interfacial entrainment rate  $U^*L/bw$  is plotted as a function of  $Fr_{int}$  in figure 5. The main point of figure 5 is that the 11 experiments from vertical plumes and density currents on  $75^\circ$  and  $90^\circ$  slopes, with a range of initial  $\Delta_{12}$ , exhibit the same trend. The values of the normalized interfacial entrainment rate  $U^*L/bw$ , the entrained buoyancy flux  $B^*$  and  $Fr_{int}$  were determined for the experiments in which there was significant deepening of the upper layer (runs 10 to 20), using the observed rate of change of depth  $\partial \hat{H}/\partial t$  and (24) in a similar manner to Kumagai (1984). The position of the interface between the upper and lower layer is found by fitting curves to the time-slice data, as shown in figure 3(c). The resulting normalized interfacial entrainment rate  $U^*L/bw$  is plotted as a function of Froude number in figure 5, and can be seen to increase steeply with Froude number. There is considerable scatter in the data and a larger range of  $Fr_{int}$  is desirable in order to seek a power-law fit with any quantitative certainty, but in order to compare these results with other measured interfacial entrainment rates found in the literature we have plotted a power-law fit to the data in figure 5 of the form  $U^*L/bw = Fr_{int}^5$ . Such an increase in entrainment rates with Froude number is consistent with previous experiments where a point-source plume strikes a two-layer interface, i.e. Ching *et al.* (1993) who measured  $U^*L/bw \sim Fr_{int}^2$ , and Baines (1975) who measured  $U^*L/bw \sim Fr_{int}^3$ . We have also made estimates of the values of the entrained buoyancy flux,  $B^* = L\Delta_{12}U^*$ . This

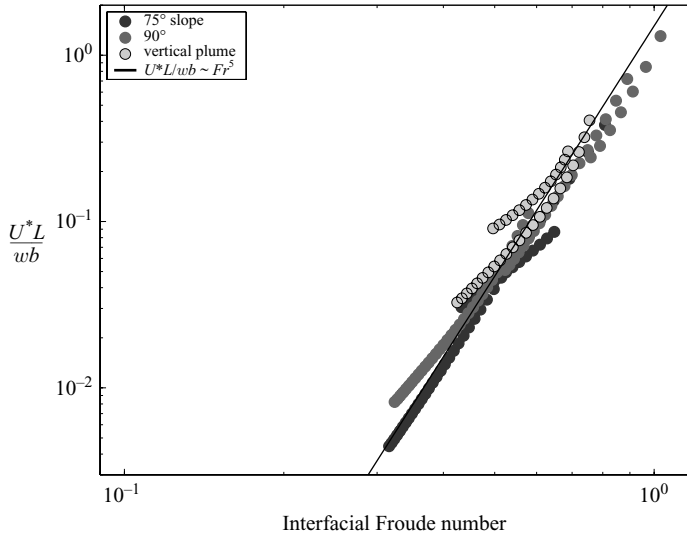


FIGURE 5. Plot of the normalized interfacial entrainment ratio  $U^*L/wb$  against the Froude number,  $Fr_{int}$  of equation (21), for runs 10–20 where there is significant entrainment for 75° and 90° slopes and free plumes. The normalized interfacial entrainment rate is seen to increase with Froude number in a manner consistent with  $U^*L/bw \propto Fr_{int}^5$ .

was done by using (24) to estimate the time-dependent  $\Delta_{12}$ , and by calculating the interfacial entrainment velocity from  $U^* = \partial \hat{H} / \partial t$ . There is considerable scatter in the resulting data, but the maximum values of  $B^*/B$  are less than 0.25, comparable with observations of Kumagai (1984) and consistent with the energetic arguments of Manins & Turner (1978).

#### 4. Application to the Arctic halocline

An important application of our work concerns the seasonal buoyancy forcing in polar oceans owing to freezing and melting. In the present climate, warm salty water enters the Arctic Ocean through the east side of Fram Strait, eventually returning as a much colder and only slightly more fresh water-mass that flows southward along the Greenland coast (Aagaard & Greisman 1975). Small variations in the fresh-water export from the upper ocean through Fram Strait, which are coupled to the seasonal ice cover, influence the stability of global thermohaline convection by modulating deep-water formation in the North Atlantic (Roach, Aagaard & Carsey 1993; Morison, Aagaard & Steele 2000; Gascard *et al.* 2002; Proshutinsky, Bourke & McLaughlin 2002; Polyakov *et al.* 2003).

The principal features of the vertical structure of the Arctic Ocean are: (i) an isothermal surface mixed layer with a seasonally dependent depth between 50 and 100 m and an isohaline surface layer with a depth of about 50 m; (ii) a distinct cold halocline between approximately 50 and 200 m depth; (iii) Warm Atlantic water that is centred between 300 and 500 m; and (iv) the abyss. We highlight three essential issues. First, Nansen noted that the halocline waters could not simply be a linear mixture of Atlantic and mixed-layer waters (e.g. Aagaard, Coachman & Carmack 1981; Carmack 2000). Secondly, shelf-derived waters and water masses associated with central basin solidification and melting are involved in the formation and maintenance of the halocline, but their relative roles, seasonal dependence and climatology remain



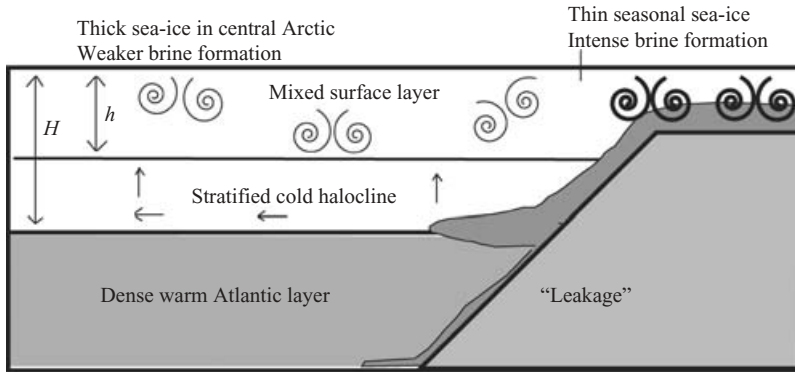


FIGURE 6. A sketch of contributions to the dynamics of halocline maintenance. Oceanic freezing and melting in the shelf regions of the Arctic Ocean, which constitute some 30 % of the basin surface area, drives seasonal buoyancy forcing. In summer, melting sea-ice and river input lead to a freshening of surface waters, creating a layer of stable stratification that acts to suppress the vigour of winter convection, driven by ice formation and brine rejection on shallow shelf regions; the resulting density current flows down the slope into the halocline. If there is a distribution of cooling over the basin, there may be a convectively mixed surface-layer over the deeper layered halocline. The upwelling of the denser stratified waters can keep the surface mixed layer from deepening (Wells & Sherman 2001).

to be explained (Aagaard *et al.* 1981; Melling & Lewis 1982; Rudels, Anderson & Jones 1996; Steele & Boyd 1998; Kikuchi, Hatakeyama & Morison 2004; Yamamoto-Kawai, Tanaka & Pivovarov 2005). Thirdly, the salinity dependence of density makes the Arctic halocline a pycnocline, and the salt stratification provides the stability required to suppress the upward flux (due to stratified turbulence) of warm waters of Atlantic origin. This stability is crucial to the persistence of a perennial sea-ice cover because there is sufficient heat below the halocline to melt the ice.

The current hypotheses of the main contributions to the formation of halocline water masses are: (a) the creation, and subsequent lateral advection into the basin, of brine-enriched waters in broad shelf regions created by oceanic freezing (Aagaard *et al.* 1981; Melling & Lewis 1982); (b) the melting of sea-ice in Fram Strait when contacting warm waters of the West Spitsbergen current and subsequent advection into the basin and convective interaction with the surface (Untersteiner 1988; Rudels *et al.* 1996); and (c) the flow of Pacific waters into the Canadian basin through the Bering Strait (Coachman & Aagaard 1988). Despite these compelling observations, and the relevance of a number of numerical and theoretical modelling studies of dense plume dynamics, with and without entrainment (e.g. Killworth 1977; Stigebrandt 1981; Björk 1989; Gawarkiewicz & Chapman 1995; Carmack & Chapman 2003), there have been relatively few laboratory studies of direct relevance to the Arctic halocline problem (e.g. Hunkins & Whitehead 1992; Whitehead 1993; Maxworthy & Narimousa 1994; Cenedese *et al.* 2004). A conceptual picture of the formation and stability of the Arctic halocline (figure 6) is in part a generalization of that put forth by Aagaard *et al.* (1981).

The essential question is: what conditions are necessary for dense shelf waters to intrude above the warmer Atlantic waters (i.e. seasonal stratification for a given buoyancy forcing), and how sensitive is this flow to changes in the location and magnitude of the seasonal buoyancy forcing? Equation (25), and hence the associated figure 4, can be used to study the issue of penetrative ventilation as follows. For the

geophysical setting we will use a value of  $Ri_\rho^* = 21$  and we consider a halocline depth of 150 m. We estimate a range of  $Ri_\rho^{in}$  by considering field data typical of both the Eurasian and Canadian basins (Aagaard *et al.* 1981; Melling & Lewis 1982) where  $0.0038 \leq \Delta_{12} \leq 0.026 \text{ m s}^{-2}$  and we take the most conservative estimate of the average buoyancy flux which derives from the argument that the fresh-water residence time of the Arctic Ocean, 10 years, is the same as that of the upper pycnocline (Aagaard *et al.* 1981). Over the area of the Arctic of  $9 \times 10^6 \text{ km}^2$  this gives a volume flux of  $2.8 \times 10^6 \text{ m}^3 \text{ s}^{-1}$  and with the weakest stratification observed by Aagaard *et al.* (1981) of  $\Delta_{12} = 0.0221 \text{ m s}^{-2}$ , we have a buoyancy flux per unit area ( $A$ ) of  $B_A = 8 \times 10^{-9} \text{ m}^2 \text{ s}^{-3}$ . Because that flux is delivered to the halocline over a basin scale  $L \approx 1000 \text{ km}$  and because  $B = B_A A / L \approx B_A L$  we have  $B = 0.008 \text{ m}^3 \text{ s}^{-3}$ . Thus, we find  $56.2 \lesssim Ri_\rho^{in} \lesssim 97.5$ , from which the penetration time is  $0.56 \lesssim t_p \lesssim 1.2$  years. Therefore, under present day stratification and conservative estimates of buoyancy forcing, it is clearly possible for gravity current penetration to occur over a time scale commensurate with the seasonality of the forcing itself.

Finally, we note that (a) because ocean freezing persists for approximately six months a year, our results indicate the possibility that penetration may occur during a seasonal time scale, and (b) both the role of rotation and regionally specific oceanographic effects will influence the detailed time scales of any penetration event. Density currents will be influenced by topography and deflected to the right in the Northern hemisphere by the Coriolis force, an effect nicely illustrated in the studies by Chao & Shaw (2003) and Cenedese *et al.* (2004). The velocity of a rotating density current is typically slower and no longer scales as (12), but rather it is determined by a balance between buoyancy forces and bottom drag. Rotation has two direct effects on the current density; for the current to fall the same vertical distance, the trajectory is longer and the velocity, and hence the entrainment rate, are reduced. The longer trajectory may balance the reduced entrainment so that the same total entrainment per unit fall may occur (as assumed by Hughes & Griffiths 2006). The entrainment dynamics of sub-critical density currents on low-angle slopes, where bottom drag is important, are not well understood (see discussion in Cenedese *et al.* 2004; Wahlin & Cenedese 2006) so it is unclear whether, for these oceanographic flows, the use of (10) necessarily implies a value of  $E_{eq}$  in the range from 0.08 to 0.1. We also note that extrapolation of equation (14) to the lower-angle slopes typical of the ocean, implies values of  $Ri_\rho^*$  less than 21. For example, using (14) with  $C = 0.2$  and  $\theta = 5^\circ$  gives  $Ri_\rho^* = 11.88$ , and hence through (25) a longer time to penetration. However, there are few experimental measurements of entrainment for slopes below  $5^\circ$ , so extrapolation to low-angle slopes to determine the exact numeric value of  $Ri_\rho^*$  is difficult. Finally, experiments and simulations on vertical convection into rotating two-layer fluids show that penetration has ostensibly no Rossby-number dependence (Narimousa 1996; Chapman 1997). However, in experiments of the type presented here but in a rotating system, we find that rotation suppresses the mixing and entrainment of density currents on a slope and hence reduces the value of  $t_p$  relative to the values found here. Moreover, during the rapid growth of sea-ice in winter, the order of magnitude of the typical buoyancy forcing associated with brine rejection is  $B_A = 10^{-7} \text{ m}^2 \text{ s}^{-3}$ , approximately an order of magnitude greater than the averaged value used in our analysis. Thus, we interpret our estimates of penetration to be conservative as regards their application to the Arctic, and we are currently trying to clarify the most important processes of geophysical relevance through rotating laboratory experiments where a dense current impinges a sharp density interface. We conclude that the general mechanism of ventilation is supported by current

oceanographic evidence and our result provides a fluid mechanical basis for the viability of the phenomenon in the Arctic.

## 5. Conclusions

We have described the underlying theory and presented experimental results of the long-term dynamics of two-dimensional density currents flowing into a two-layer stratified basin. We find that a density current will penetrate the initial stratification if the initial Richardson number, defined here as  $Ri_\rho^{in} = \Delta_{12}^{in} H / B^{2/3}$ , is less than  $Ri_\rho^* = 21 - 27$  for slopes between  $30^\circ$  and  $90^\circ$ . Experimentally, we find that this result is independent of slope angle, because the total entrainment of a density current on a slope is the same as an equivalent vertical plume falling the same vertical depth (Hughes & Griffiths 2006; Wells & Wettlaufer 2005). If the density current does not initially penetrate the interface, then the density contrast between the two layers reduces with time. The time scale for penetration of the interface is given by  $t_p = (Ri_\rho^{in} - Ri_\rho^*)L / B^{1/3}$  and again does not depend upon the slope angle within experimental uncertainty. A principal experimental observation is that there appears to be no appreciable penetrative convection for density currents on slopes less than  $75^\circ$ , even though the interfacial Froude numbers on a wide range of slopes are in the same range. We attribute this transition in the vigour of the penetrative convection to a transition in the form of the hydraulic jump at the point where the fast down-slope density current transitions to a slower intruding current. In experiments with low slopes, this hydraulic jump has the form an undular bore and there is little entrainment at the interface, whereas with steep slopes and higher values of the overall Froude number, the hydraulic jump has the form of a strongly entraining turbulent bore.

Finally, the stability of the Arctic halocline, which presently insulates the sea-ice from deeper warmer waters of Atlantic origin, can be understood in the context of these experiments. The halocline waters originate from cold dense saline currents driven by brine rejection into the shelf regions of the Arctic. If a density current could penetrate through the interface it would gradually bring the warmer Atlantic waters into contact with the surface sea-ice by a combination of upwelling, on a slower filling-box time scale, and the erosion of the existing stratification, which on a faster time scale allows the surface forcing to penetrate more deeply into the water column. For a range of the present oceanographic conditions, we have used equation (25) to estimate the penetration time scale,  $t_p$ , and find  $0.56 \lesssim t_p \lesssim 1.2$  years. Hence, we find that gravity current penetration may transpire on a time scale of the order of the seasonal buoyancy forcing.

The authors are very grateful for conversations with C. Caulfield, C. Cenedese, R. W. Griffiths, H. E. Huppert, J. J. Monaghan, L. J. Pratt, M.-L. Timmermans, G. Veronis and M. G. Worster. We thank M. G. Worster for a critical reading of the manuscript and the referees for their comments and criticism. We acknowledge NSF OPP-0440841 and Yale University for support. J. S. W. thanks Trinity College and the Department of Applied Mathematics and Theoretical Physics, University of Cambridge, for support during the sabbatical leave when this paper was written.

## REFERENCES

- AAGAARD, K. & GREISMAN, P. 1975 Toward new mass and heat budgets for the Arctic Ocean. *J. Geophys. Res.* **80**, 3821–3827.

- AAGAARD, K., COACHMAN, L. K. & CARMACK, E. C. 1981 On the halocline of the Arctic Ocean. *Deep-Sea Res.* **28**, 529–545.
- BAINES, P. G. 1995 Topographic effects in fluids. *Cambridge University Press*.
- BAINES, P. G. 2001 Mixing in flows down gentle slopes into stratified environments. *J. Fluid Mech.* **443**, 237–270.
- BAINES, P. G. 2005 Mixing regimes for the flow of dense fluid down slopes into stratified environments. *J. Fluid Mech.* **538**, 245–267.
- BAINES, W. D. 1975 Entrainment by a plume or jet at a density interface. *J. Fluid Mech.* **68**, 309–320.
- BAINES, W. D. & TURNER, J. S. 1969 Turbulent buoyant convection from a source in a confined region. *J. Fluid Mech.* **37**, 51–80.
- BARINGER, M. O. & PRICE, J. F. 1999 A review of the physical oceanography of the Mediterranean outflow. *Marine Geol.* **155**, 63–82.
- BJÖRK, G. 1989 A one-dimensional time-dependent model for the vertical stratification of the upper Arctic Ocean. *J. Phys. Oceanogr.* **19**, 52–67.
- BRIGGS, G. A. 1969 Plume rise. *US Atomic Energy Commission Critical Review Series*. TID-25075.
- BRITTER, R. F. & LINDEN, P. F. 1980 The motion of the front of a gravity current travelling down an incline. *J. Fluid Mech.* **99**, 531–543.
- BUSH, J. W. M. & WOODS, A. W. 1999 Vortex generation by line plumes in a rotating stratified fluid. *J. Fluid Mech.* **388**, 289–313.
- CARDOSO, S. S. S. & WOODS, A. W. 1993 Mixing by a turbulent plume in a confined stratified region. *J. Fluid Mech.* **250**, 277–305.
- CARMACK, E. C. 2000 The Arctic Ocean's freshwater budget: sources, sinks and export. In *The Freshwater Budget of the Arctic Ocean* (ed. E. L. Lewis, E. P. Jones, P. Lemke, T. D. Prowse, & P. Wadhams), pp. 91–126. Kluwer.
- CARMACK, E. C. & CHAPMAN, D. C. 2003 Wind-driven shelf/basin exchange on an Arctic shelf. The joint roles of ice cover extent and shelf-break bathymetry. *Geophys. Res. Lett.* **30**, 1778, doi:10.1029/2003GL017755.
- CAULFIELD, C. & WOODS, A. W. 1998 Turbulent gravitational convection from a point source in a non-uniformly stratified environment. *J. Fluid Mech.* **360**, 229–248.
- CENEDESE, C., WHITEHEAD, J. A., ASCARELLI, T. A. & OHIWA, M. 2004 A dense current flowing down a sloping bottom in a rotating fluid. *J. Phys. Oceanogr.* **34**, 188–203.
- CHAO, S. Y. & SHAW, P. T. 2003 A numerical study of dense water outflows and halocline anticyclones in an Arctic baroclinic slope current. *J. Geophys. Res.* **108**, 3226, doi:10.1029/2002JC001473.
- CHAPMAN, D. C. 1997 A note on isolated convection in a rotating two-layer fluid. *J. Fluid Mech.* **348**, 319–325.
- CHING, C. Y., FERNANDO, H. J. S. & NOH, Y. 1993 Interaction of a negatively buoyant line plume with a density interface. *Dyn. Atmos. Oceans* **19**, 367–388.
- CHOW, V. T. 1959 *Open-Channel Hydraulics*. McGraw-Hill.
- COACHMAN, L. K. & AAGAARD, K. 1988 Transports through Bering Strait; annual and inter-annual variability. *J. Geophys. Res.* **93**, 15 535–15 539.
- COTEL, A. J. & BREIDENTHAL, R. E. 1997 Jet detrainment at a stratified interface. *J. Geophys. Res.* **102**, 23 813–23 818.
- COTEL, A. J., GJESTVANG, J. A., RAMKHELAWAN, N. N. & BREIDENTHAL, R. E. 1997 Laboratory experiments of a jet impinging on a stratified interface. *Exps. Fluids* **23**, 155–160.
- ELLISON, T. H. & TURNER, J. S. 1959 Turbulent entrainment in stratified flows. *J. Fluid Mech.* **6**, 423–448.
- FISCHER, H. B., LIST, E. J., KOH, R. C. Y., IMBERGER, J. & BROOKS, N. H. 1979 *Mixing in Coastal and Inland Waters*. Academic.
- GASCARD, J. C., WATSON, A. J., MESSIAS, M., OLSSON, K. A., JOHANNESSEN, T. & SIMONSENK, K. 2002 Long-lived vortices as a mode of deep ventilation in the Greenland Sea. *Nature* **416**, 525–527.
- GAWARKIEWICZ, G. & CHAPMAN, D. C. 1995 A numerical study of dense water formation and transport on a shallow, sloping continental shelf. *J. Geophys. Res.* **100**, 4489–4507.
- HAMBLIN, P. F. & CARMACK, E. C. 1978 River induced currents in a Fjord lake. *J. Geophys. Res.* **83**, 885–899.
- HEBBERT, B., IMBERGER, J., LOH, I. & PATTERSON, J. 1979 Collie river underflow into the Wellington reservoir. *J. Hydraul. Div. ASCE* **105**, 533–545.

- HUGHES, G. O. & GRIFFITHS, R. W. 2006 A simple convective model of the global overturning circulation, including effects of entrainment into sinking regions. *Ocean Model.* **12**, 46–79.
- HUNKINS, K. & WHITEHEAD, J. A. 1992 Laboratory simulation of exchange through Fram Strait. *J. Geophys. Res.* **97**, 11 299–11 321.
- IMBERGER, J. & HAMBLIN, P. F. 1982 Dynamics of lakes, reservoirs, and cooling ponds. *Annu. Rev. Fluid. Mech.* **14**, 153–187.
- KIKUCHI, T., HATAKEYAMA, K. & MORISON, J. H. 2004 Distribution of convective Lower Halocline Water in the eastern Arctic Ocean. *J. Geophys. Res.* **109**, C12030, doi:10.1029/2003JC002223.
- KILLWORTH, P. D. 1977 Mixing on the Weddell Sea continental slope. *Deep-Sea Res.* **24**, 427–448.
- KILLWORTH, P. D. & CARMACK, E. C. 1979 A filling box model of river dominated lakes. *Limnol. Oceanogr.* **24**, 201–217.
- KNELLER, B. C., BENNETT, S. J. & MCCAFFREY, W. D. 1999 Velocity structure, turbulence and fluid stresses in experimental gravity currents. *J. Geophys. Res.* **104**, 5381–5391.
- KULKARNI, A. C., MURPHY, F. & MANOHAR, S. S. 1993 Interaction of buoyant plumes with two-layer stably stratified media. *Expl Thermal Fluid Sci.* **7**, 241–248.
- KUMAGAI, M. 1984 Turbulent buoyant convection from a source in a confined two-layered region. *J. Fluid Mech.* **147**, 105–131.
- MANINS, P. C. & TURNER, J. S. 1978 The relation between flux ratio and energy ratio in convectively mixed-layers. *Q. J. R. Met. Soc.* **104**, 3944.
- MARINO, B. M., THOMAS, L. P. & LINDEN, P. F. 2005 The front condition for gravity currents. *J. Fluid Mech.* **536**, 49–78.
- MAXWORTHY, T. & NARIMOUSA, S. 1994 Unsteady, turbulent convection into a homogeneous, rotating fluid, with oceanographic applications. *J. Phys. Oceanogr.* **24**, 865–887.
- MELLING, H. & LEWIS, E. L. 1982 Shelf drainage flows in the Beaufort Sea and their effect on the Arctic Ocean pycnocline. *Deep-Sea Res.* **29**, 967–985.
- MONAGHAN, J. J., CAS, R. A. F., KOS, A. M. & HALLWORTH, M. A. 1999 Gravity currents descending a ramp in a stratified tank. *J. Fluid Mech.* **379**, 39–70.
- MORISON, J. H., AAGAARD, K. & STEELE, M. 2000 Recent environmental changes in the Arctic: a review. *Arctic* **53**, 359–371.
- MORTON, B. R., TAYLOR, G. I. & TURNER, J. S. 1956 Turbulent gravitational convection from maintained and instantaneous sources. *Proc. R. Soc. Lon. A* **234**, 1–32.
- NARIMOUSA, S. 1996 Penetrative turbulent convection into a rotating two-layer fluid. *J. Fluid Mech.* **321**, 299–313.
- NOH, Y., FERNANDO, H. J. S. & CHING, C. Y. 1992 Flows induced by the impingement of a two-dimensional thermal on a density interface. *J. Phys. Oceanogr.* **22**, 1207–1222.
- POLYAKOV, I., WALSH, D., DMITRENKO, I., COLONY, R. & TIMOKHOV, L. A. 2003 Arctic Ocean variability derived from historical observations. *Geophys. Res. Lett.* **30**, doi:10.1029/2001GL016441.
- PROSHUTINSKY, A., BOURKE, R. H. & MCLAUGHLIN, F. A. 2002 The role of the Beaufort Gyre in Arctic climate variability: seasonal to decadal climate scales. *Geophys. Res. Lett.* **29**, doi:10.1029/2001GL015847.
- ROACH, A. T., AAGAARD, K. & CARSEY, F. D. 1993 Coupled ice-ocean variability in the Greenland Sea. *Atmos.-Ocean* **31**, 319–337.
- RUDELS, B., ANDERSON, L. & JONES, E. 1996 Formation and evolution of the surface mixed-layer and Halocline of the Arctic Ocean. *J. Geophys. Res.* **101**, 8807–8822.
- SHIN, J. O., DALZIEL, S. B. & LINDEN, P. F. 2004 Gravity currents produced by lock exchange. *J. Fluid Mech.* **521**, 1–34.
- STEELE, M. & BOYD, T. 1998 Retreat of the cold halocline layer in the Arctic Ocean. *J. Geophys. Res.* **103**, 10419–10435.
- STIGEBRANDT, A. 1981 A model for the thickness and salinity of the upper layer in the Arctic Ocean and the relationship between the ice thickness and some external parameters. *J. Phys. Oceanogr.* **11**, 1407–1422.
- STOMMEL, H. 1958 The abyssal circulation. *Deep-Sea Res.* **5**, 80–82.
- SUKRU, B., OZSOY, E. & UNLUATA, U. 1993 Filling of the Marmara Sea by the Dardanelles lower layer inflow. *Deep-Sea Res.* **40**, 1815–1838.

- TAYLOR, G. I. 1948 Dynamics of a mass of hot gas rising in air. *USAEC Rep. MDDC-919 (LADC-276)*, Los Alamos Scientific Laboratory, National Technical Information Service, Springfield, VA.
- TURNER, J. S. 1973 *Buoyancy Effects in Fluids*. Cambridge University Press.
- TURNER, J. S. 1986 Turbulent entrainment – the development of the entrainment assumption and its application to geophysical flows. *J. Fluid. Mech.* **173**, 431–471.
- UNTERSTEINER, N. 1988 On the ice and heat balance in Fram Strait. *J. Geophys. Res.* **93**, 527–531.
- WAHLIN, A. K. & CENEDESE, C. 2006 How entraining density currents influence the ocean stratification in a one-dimensional ocean basin. *Deep-Sea Res. II* **53**, 172–193.
- WALLACE, R. B. & SHEFF, B. 1987 Two-dimensional buoyant-jets in two-layer ambient fluid. *J. Hydraulic Engng ASCE* **113**, 992–1005.
- WELLS, M. G. & SHERMAN, B. 2001 Stratification produced by surface cooling in lakes with significant shallow regions. *Limnol. Oceanogr.* **46**, 1747–1759.
- WELLS, M. G. & WETTLAUFER, J. S. 2005 Two-dimensional density currents in confined basins. *Geophys. Astrophys. Fluid Dyn.* **99**, 199–218.
- WHITEHEAD, J. A. 1993 A laboratory model of cooling over the continental shelf. *J. Phys. Oceanogr.* **23**, 2412–2427.
- WORSTER, M. G. & HUPPERT, H. E. 1983 Time-dependent density profiles in a filling box. *J. Fluid. Mech.* **132**, 457–466.
- WRIGHT, S. J. & WALLACE, R. B. 1979 Two-dimensional buoyant jets in stratified fluid. *J. Hydraul. Div. ASCE* **105**, 1393–1406.
- YAMAMOTO-KAWAI, M., TANAKA, N. & PIVOVAROV, S. 2005 Freshwater and brine behaviors in the Arctic Ocean deduced from historical data of  $\delta O_{18}$  and Alkalinity (1929–2002 AD). *J. Geophys. Res.* **110**, doi:10.1029/2004JC002793.